Estimation of Hydraulic Conditions of Tsunami from Deposits: Inverse Model using Deep-Learning Neural Network

Rimali Mitra[1,1], Hajime Naruse[1,1], and Tomoya Abe[2,2]

[1]Kyoto University
[2]Geological Survey of Japan, AIST

November 30, 2022

Abstract

Tsunami deposits provide information for estimating the magnitude and flow conditions of paleotsunamis, and inverse models have potential for reconstructing hydraulic conditions of tsunamis from their deposits. The majority of the previously proposed models are based on oversimplified assumptions and possess some limitations. We present a new inverse model based on the FITTNUSS model, which incorporates nonuniform and unsteady transport of suspended sediment and turbulent mixing. The present model uses a deep neural network (DNN) for the inversion method. In this method, forward model calculations are repeated for random initial flow conditions (e.g., maximum inundation length, flow velocity, maximum flow depth and sediment concentration) to produce artificial training data sets of depositional characteristics such as thickness and grain size distribution. The DNN was then trained to establish a general inverse model based on artificial data sets derived from the forward model. Tests conducted using independent artificial data sets indicated that this trained DNN can reconstruct the original flow conditions from the characteristics of the deposits. Finally, the model was applied to a data set of 2011 Tohoku-Oki tsunami deposits. The predicted results of flow conditions were verified by the observational records at Sendai plain. Jackknife resampling was applied to estimate the precision of the result. The estimated results of the flow velocity and maximum flow depth were approximately 5.4\pm0.140 m/s and 4.11\pm0.152 m, respectively after the uncertainty analysis. The DNN shows promise for reconstruction of tsunami characteristics from its deposits, which would help in estimating the hydraulic conditions of paleotsunamis.

Estimation of Tsunami Characteristics from Deposits: Inverse Modeling using a Deep-Learning Neural Network

Rimali Mitra[1], Hajime Naruse[1], and Tomoya Abe[2]

[1]Division of Earth and Planetary Sciences, Graduate School of Science, Kyoto University, Kitashirakawa Oiwakecho, Kyoto, Japan.

[2]Research Institute of Geology and Geoinformation, Geological Survey of Japan, National Institute of Advanced Industrial Science and Technology (AIST), AIST, Tsukuba, Japan.

Contents of this file

1. Table S1
2. Table S2

Additional Supporting Information (Files uploaded separately)

1. Table S1: 2011 Tohoku-Oki Tsunami at Sendai plain data set for six grain size classes
2. Table S2: Influence of friction coefficient (c_f) and different number grain size class on the inverse model

Introduction

The auxiliary material consists of Table S1. The tsunami deposit was measured and sampled during a field survey conducted 3 months after the tsunami event that occurred on 11th March 2011. The samples were collected along 4.02 km long transect from the shoreline to the inundation limit in the northern part of Sendai plain. This transect was almost perpendicular to the shoreline. The tsunami deposit was sampled at the 27 locations along the transect.

June 7, 2020, 5:34pm

Estimation of Tsunami Characteristics from Deposits: Inverse Modeling using a Deep-Learning Neural Network

Rimali Mitra[1], Hajime Naruse[1], and Tomoya Abe[2]

[1]Division of Earth and Planetary Sciences, Graduate School of Science, Kyoto University, Kitashirakawa Oiwakecho, Kyoto, Japan.

[2]Research Institute of Geology and Geoinformation, Geological Survey of Japan, National Institute of Advanced Industrial Science and Technology (AIST), Tsukuba, Japan.

Key Points:

- Inverse modeling of paleotsunami deposits was performed using deep learning neural networks.
- 2011 Tohoku-Oki tsunami's flow velocity, maximum depth and inundation length, and sediment concentration were evaluated with inverse model.
- Comparison of observations and uncertainty analysis implied that the reconstructed flow conditions were accurate and reasonably precise.

Corresponding author: Rimali Mitra, mitra.rimali.37z@st.kyoto-u.ac.jp

Abstract

Tsunami deposits provide information for estimating the magnitude and flow conditions of paleotsunamis, and inverse models have potential for reconstructing hydraulic conditions of tsunamis from their deposits. The majority of the previously proposed models are based on oversimplified assumptions and possess some limitations. We present a new inverse model based on the FITTNUSS model, which incorporates nonuniform and unsteady transport of suspended sediment and turbulent mixing. The present model uses a deep neural network (DNN) for the inversion method. In this method, forward model calculations are repeated for random initial flow conditions (e.g., maximum inundation length, flow velocity, maximum flow depth and sediment concentration) to produce artificial training data sets of depositional characteristics such as thickness and grain size distribution. The DNN was then trained to establish a general inverse model based on artificial data sets derived from the forward model. Tests conducted using independent artificial data sets indicated that this trained DNN can reconstruct the original flow conditions from the characteristics of the deposits. Finally, the model was applied to a data set of 2011 Tohoku-Oki tsunami deposits. The predicted results of flow conditions were verified by the observational records at Sendai plain. Jackknife resampling was applied to estimate the precision of the result. The estimated results of the flow velocity and maximum flow depth were approximately 5.4±0.140 m/s and 4.11±0.152 m, respectively after the uncertainty analysis. The DNN shows promise for reconstruction of tsunami characteristics from its deposits, which would help in estimating the hydraulic conditions of paleotsunamis.

Plain Language Summary

This study presents an inverse model that uses an artificial intelligence technique to estimate the hydraulic conditions of paleotsunamis from deposits.

1 Introduction

Tsunamis are one of the most disastrous natural hazards that occur in coastal zones. They are a threat to the overall socio-economic infrastructure of coastal-based cities (Lin et al., 2012). Tsunami hazard assessment is necessary for any fast-growing coastal city. The 2004 Indian Ocean tsunami and 2011 Tohoku-Oki tsunami caused devastating damage to many Asian countries, but such situations are worsened when countries lack tsunami-

related preparedness for disasters that cause human causalities and extensive building damage (Imamura et al., 2019). Ghobarah et al. (2006) reported that the debris carried by the 2004 Indian Ocean tsunami could cause major building damage. The 2004 Indian Ocean tsunami caused extensive structural and non-structural destruction of reinforced concrete buildings (Saatcioglu et al., 2005).

To mitigate tsunami disasters, a method of inverse modeling of tsunamis based on their geologic records has been developed. Tsunami deposits are defined as layers of sediment formed by hydrodynamic activities of tsunami, and research on tsunami deposits started since early 1950s (Shephard et al., 1950; Bourgeois et al., 2009).

The mode of sediment transportation and deposition by tsunamis can be understood via a detailed study of tsunami deposits (Costa et al., 2015). Also, several studies of forward modeling as well as flume experiments of tsunamis have successfully reproduced features of tsunami deposits observed in field surveys (Johnson et al., 2016; Li et al., 2012; Sugawara et al., 2012; Yoshii et al., 2018). Using this knowledge, a quantitative reconstruction of environmental conditions such as flow velocity and maximum flow depth has been attempted using several inverse modeling approaches (Soulsby, 1997; Jaffe & Gelfenbuam, 2007; Jaffe et al., 2012; Tang & Weiss, 2015).

However, previous studies on inverse modeling were based on forward models using unreasonably simplified assumptions. For example, in the settling-advection model (or moving-settling tube model), it was assumed that all the sediment particles settle in the water column without any turbulent mixing, resuspension or subsequent erosion (Soulsby et al., 2007; Moore et al., 2007; Jaffe & Gelfenbuam, 2007). Tang and Weiss (2015) assumed that sediment suspension in tsunamis occurs under uniform and steady conditions and uprush stops suddenly. As a result, situations to which these inverse models are applicable are quite limited (Jaffe et al., 2016; Naruse & Abe, 2017). Moore et al. (2007) proposed a point inverse model based on advection settling of large particles in deposit, wherein the settling velocities of the larger particles (D_{84} and D_{100}) in the deposit were used as input data, and the model estimated the average flow speed of the tsunami inundation. Moore et al. (2007) assumed that sediment grains travel without diffusion in water column and are not resuspended from bed, and thus a trajectory of a single grain is supposed to be linear. However, the movements of sediment grains do not obey such linear trajectory but they travel considerably longer distances because of

the flow turbulence (Braaten et al., 1990). Under the assumption of a linear trajectory, very large flow velocity is required to explain the travel distance that was actually observed. Indeed, Sugawara (2014) indicated from the field measurements that their advection-settling assumption cannot be justified in the case of 2011 Tohoku-Oki tsunami. D. Smith et al. (2007) proposed another point model based on particle settlings but only the finest grain size classes of 106–184 μm were used in this model; however, the incorporation of larger grain size classses is essential for obtaining accurate estimation from tsunami deposits (Naruse & Abe, 2017). In contrast, Soulsby et al. (2007) proposed the 1D model that deciphered the run-up elevation and inundation distance, Although sediment dynamics and optimization of input parameters were considered, no resuspension process of sediment particles was incorporated in the model assumption, so that significant overestimation of the flow velocity also occurs similar to the method of Moore et al. (2007). Jaffe and Gelfenbuam (2007) presented a point model (TsuSedMod) using the thickness and bulk grain size distribution of suspension-graded intervals of tsunami deposits to estimate the maximum tsunami flow speed, This model assumes that sediment deposited was is in a suspension that was in equilibrium with the maximum flow speed. See Jaffe et al. (2012) for model details. This model does not consider the temporal variation of deceleration of the flow. Thus, the application of TsuSedMod is limited to the study areas where only the condition of uniform and steady tsunami flow is supposed to be approached. The application of TsuSedMod involves, the spliting of tsunami deposits into two parts: the lower part deposited from run-up flow and the upper part deposited from the stagnant water. This interpretation is not always easy because both parts may be normally graded. Non-uniform sediment transport cannot be considered in this model. The estimation of flow velocity can be strongly affected by the assumptions mentioned above. Moreover, additional input information such as flow depth was required for the model (Naruse & Abe, 2017). Choowong et al. (2008) applied TsuSedMod to two units around Bangtao Beach, Phuket, Thailand and obtained an extremely high estimate of 2004 Indian Ocean tsunami flow velocities (19–21 m/s), although a reason for this overestimation of flow velocity can be that they used mean grain size instead of the entire grain size distribution in their analysis.

To resolve issues in previous inverse models, the inverse model FITTNUSS (Naruse & Abe, 2017) was proposed, in which a forward model for calculating sediment hydrodynamics and nonuniform, unsteady suspended sediment transport processes during run-

up and stagnant phases was employed. The overall computational and calculation efficiency was increased by using a transformed coordinate system of moving boundary type in the forward model. The inverse model requires the spatial variation of thickness and grain size distribution of the tsunami deposit along 1D shoreline-normal transects. It has ability to produce flow conditions such as run-up flow velocity, maximum flow depth and sediment concentration. However, the model still had many limitations such as poor performance of the model with increasing amount of data and grain size classes due to the optimization procedures of parameters during inversion. This model employed limited memory Broyden-Fletcher-Goldfarb-Shanno (LBFGS) method to optimize the flow conditions in the forward model for minimizing difference between observations and model results (Naruse & Abe, 2017). This is a kind of quasi-Newtonian algorithm but it requires the gradient of the objective function that can be obtained only by numerical method and tedious trial and error iterations are needed for calculation. Also, it may find local minimum solutions depending on the starting values of calculation so that multiple iterations with different starting values are needed. As a result, it was difficult to deal with larger amount of data sets, and it was impossible to use uncertainty analyses because computational statistical methods, such as the jackknife method, require iterations of an inverse analysis. A brief description of jackknife method is given in the Appendix A.

In this study, we present a new inversion method that uses the use of a deep neural network (DNN) (Romano et al., 2009). This inverse model incorporates the same forward model used in FITTNUSS (Naruse & Abe, 2017). In this new methodology, however, the initial conditions and model parameters of the forward model are not optimized to fit the observed characteristics of tsunami deposits. Instead, the forward model calculation was simply repeated at random initial flow conditions (e.g., maximum inundation length, maximum flow depth, flow velocity, and sediment concentration) to produce artificial training data sets that represent artificial depositional characteristics such as the spatial distribution of thickness and grain size composition. The DNN was then trained to establish a relation between the characteristics of deposits and flow conditions based on artificial data sets. The established DNN can instantaneously predict the probable flow conditions from deposits, such that it works as an inverse model based on the tsunami deposits. The performance of the model was verified using training and test data sets. Finally, this 1D model was applied to the 2011 Tohoku-Oki tsunami deposits from the Sendai plain, and a fair prediction of the flow velocity, maximum flow depth, and con-

centration of six grain size classes was obtained. The data set of Sendai plain was selected because it is one of the best preserved data set in the history of tsunami deposits, nevertheless further reliability check of the model should be examined with other data sets as well in future studies. The precision of the model was checked using the jackknife method (Appendix A). The methodology and result were compared with the FITTNUSS model and the actual initial flow conditions. The comparison shows promise for the use of DNN as a tsunami hazard assessment tool.

2 Model Formulation

This DNN inverse model uses the forward model of FITTNUSS (Naruse & Abe, 2017) to calculate the sediment transport and deposition from the depth averaged flow velocity, the maximum flow depth, and initial sediment concentration. The forward model can reproduce the thickness and grain size distribution along a 1D shoreline normal transect, which is used to train the DNN inverse model. Our assumption in the forward model is that the topography can be approximated as flat, so that the local topographic change is not considered in the model (Naruse & Abe, 2017).

2.1 Forward model

The FITTNUSS forward model is used in the present inverse model framework. The forward model is based on the layer averaged shallow-water equations, although they are simplified in order to treat the hydraulics of tsunamis. The model calculates the spatial variation of the thickness and grain size distribution of the tsunami deposit from input values of (1) maximum distance of horizontal run-up, (2) maximum inundation depth, (3) run-up velocity, and (4) sediment concentration of each grain size class (Naruse & Abe, 2017). Here, we present a brief review of FITTNUSS forward model. (see Naruse and Abe (2017) for details). In the FITTNUSS model, shallow layer-averaged one-dimensional equations are used, which take the following form:

$$\frac{\partial h}{\partial t} + \frac{\partial Uh}{\partial x} = 0, \tag{1}$$

$$\frac{\partial Uh}{\partial t} + \frac{\partial U^2 h}{\partial x} = ghS - \frac{1}{2} g \frac{\partial h^2}{\partial x} - u_*^2. \tag{2}$$

where t and x are considered as the time and bed-attached streamwise coordinate which is, perpendicular to the shoreline and is positive landward side. Here, h refers to the tsunami inundation depth, and U is the flow velocity. The gravitational acceleration is denoted as g, S is the bed slope and u_* is the friction velocity.

The sediment conservation equation of tsunami is given as follows:

$$\frac{\partial C_i h}{\partial t} + \frac{\partial U C_i h}{\partial x} = w_{si}(F_i E_{si} - r_{0i} C_i). \tag{3}$$

In the above equation, C_i refers to the volume concentration in the suspension of the ith grain size class. The parameters w_{si}, E_{si}, r_{0i}, and F_i represent settling velocity, sediment entrainment coefficient, ratio of near-bed to layer-averaged concentration of the ith grain size class and volumetric fraction of the sediment particles in the bed surface active layer above the substrate respectively (Hirano, 1971). Several empirical functions are required to close equations such as (1), (2) and (3) for evaluating friction velocity (u_*). A detailed review of equations involving parameters in closure equations such as thickness of the active layer (L_a) (Yoshikawa & Watanabe, 2008), Shield's dimensionless shear stress (τ_{*m}), settling velocity (w_{si}) (Dietrich, 1982), sediment entrainment coefficient (E_{si}) (Rijn, 1984), correction of damping effects (ψ_i) (Rijn, 1984), are given in Naruse and Abe (2017).
.

For the sedimentation of tsunamis, the Exner equation of bed sediment continuity is used:

$$\frac{\partial \eta_i}{\partial t} = \frac{1}{1-\lambda_p} w_{si}(r_{0i} C_i - F_i E_{si}). \tag{4}$$

Here η_i refers to the volume per unit area (thickness) of the sediments of the ith grain size class accounts for the porosity of the bed sediment λ_p. As a result of the sedimentation, the grain size distribution in the active layer varies with time (Hirano, 1971), which is expressed as follows:

$$L_a \frac{\partial F_i}{\partial t} = \frac{\partial \eta_i}{\partial t} - F_i \frac{\partial \eta}{\partial t}, \tag{5}$$

Thus, the rate of total sedimentation is as follows:

$$\frac{\partial \eta}{\partial t} = \sum \frac{\partial \eta_i}{\partial t}. \tag{6}$$

Equations (4) to (6) were solved using the two step Adams-Bashforth scheme and the predictor-corrector method. Finally, the flow dynamics of tsunamis was simplified using the assumptions proposed by Soulsby et al. (2007), while considering the velocity of tsunami run-up flow as uniform and steady but that the flow depth varies with time; thus, the model is based on a quasi-steady flow assumption. The simplified equation is as follows:

$$\frac{\partial C_i}{\partial t} + U\frac{\partial C_i}{\partial x} = \frac{R_w}{H\left(Ut - x\right)}\left\{w_{si}\left(F_i E_{si} - r_{0i} C_i\right)\right\}. \tag{7}$$

where R_w and H indicate maximum inundation length and Maximum flow depth of the tsunami at the seaward (upstream) boundary of the transect, respectively.

In addition to these formulations, a transformed coordinate system (Crank, 1984) has been applied to equation (7) to increase the computational efficiency of the forward model. The implicit Euler method was used to solve the equation after applying coordinate transformation. The entire forward and inverse model were implemented using Python with the Numpy and Scipy libraries.

2.2 Inverse model

Although artificial neural networks have been primarily applied for learning observational data sets for constructing predictive models (Ramirez et al., 2005), in this study, they are used for learning the results of a numerical simulation to construct an inverse model. First, artificial training data sets are prepared by repetition of the forward model. Multiple flow conditions such as maximum inundation length, flow velocity and maximum flow depth and boundary conditions are generated randomly with a range that is possible values in natural environments. Using the generated flow conditions, the forward model calculates the grain size and thickness distributions along 1D shore-normal transect. Thus, this procedure results in multiple combinations of flow conditions and their consequences (i.e. grain size and thickness distribution of tsunami deposits), which are used for training and verification of the inverse model. Results of the forward model calculations (Figure 1) are given to an input layer of the NN. The nodes in the input layer

receive the values of the volume per unit area of each grain size class at grid cell used in the forward model. The feed-forward calculation through several hidden layers is then performed, in which the values at the nodes were summated with weighting coefficients that are assigned on connections to nodes in the next layer, and the computed total input data passes through the activation functions to produce the net output. The number of hidden layers was set to maximize the model performance (S. Smith, 2013). As a result of this feed-forward calculation, the values obtained from the output nodes provide estimates of the hydraulic conditions of tsunamis that formed the deposits. This procedure results in the training of the model followed by testing of the model performance. 20% of the artificial data is used to validate the model performance during training. If the model tends to overlearn, the selection of hyperparameters and the optimization method is required to be revised. After the model training with artificial data set is completed, the model is ready for application to a natural data set; however, the model performed training based on artificial data with set spacing.

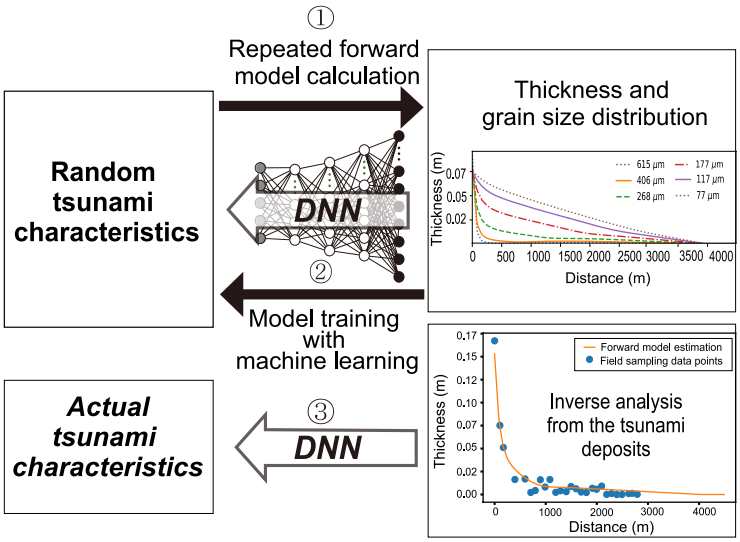

Figure 1. Workflow of the DNN inverse model.

2.2.1 Procedures for training of the inverse model

Here, we describe the procedures used for generating a training data set and the preprocessing. In the present study, in the forward model, the grain size distribution was discretized into six grain size classes, and the number of spatial computational grids in

the transformed coordinate was 50. The number of spatial grid sizes in the fixed coordinates depends on the size of the sampling window. It is important to determine the appropriate number of training data sets produced by the forward model in order to improve the inverse model training (Jordan & Rumelhart, 1992). In this study, the number of iterations of the forward model calculation was incrementally increased, and the relation between the number of training data sets and the performance of the inverse model was investigated. The range of the inundation lengths, flow velocities, maximum flow depths, and sediment concentrations used for generating the training data set is described later. The sampling window was then set to the artificial training data sets before starting the training of the DNN, and only the data in the sampling window was used for the training. This sampling window was necessary because (1) the tsunami deposit becomes too thin to measure precisely and predict computationally inland, and (2) field measurements along transects typically do not cover the entire distribution of tsunami deposits . Very-thin and finegrained tsunami deposits far inland are not easily differentiated from the background soil, and thus, the region of analysis should be limited to a relatively proximal area wherein coarser and thicker deposits are distributed. Therefore, the specific window is preferably at the proximal to middle part of the transect. As in the settings of our inverse model, the grid spacing has been maintained at a constant value of 15 m in our model. The number of grid points in the fixed coordinate varies according to the selected interval of the sampling window. After the production of the training data set and extraction of the sampling window, the normalization of the input and teacher values was performed, which is one of the most important processes in training the neural network. As the input and teaching data have largely a different range of values from each other, the normalization of the values is required to be performed to remove the computational biases towards a specific dimension of data (Bishop et al., 1995). In this case, the maximum inundation length has a larger range of values, while the values of concentration are very low. Thus, the raw values of the teaching data may predict the inundation length preferentially, while the concentration values tend to be ignored. Therefore, both the input and teaching data in the artificial data set produced by the forward model were normalized before they were given as input to the inverse model. The input data (volume per unit area of deposits) were normalized using the following equation:

$$X_{norm} = \frac{X_{raw} - \min(X_{raw})}{\max(X_{raw}) - \min(X_{raw})} \tag{8}$$

where X_{norm} and X_{raw} are the normalized and original values of the input data respectively. $\min(X_{raw})$ and $\max(X_{raw})$ denote the minimum and maximum values of the raw input data, respectively. Similarly, the teaching data that was the original conditions used in the forward model calculation was normalized using the following equation:

$$Y_{norm} = \frac{Y_{raw} - \min(Y_{raw})}{\max(Y_{raw}) - \min(Y_{raw})} \tag{9}$$

where Y_{norm} and Y_{raw} are the normalized and original values of the teaching data respectively. $\min(Y_{raw})$ and $\max(Y_{raw})$ denote the minimum and maximum values respectively, of raw teaching data. After the training, the NN outputs the normalized values of the hydraulic conditions, such that these values were converted to values in the original scale.

Then, the training and teaching data set were given to the NN for training. The overall neural network structure consists of three parts, the input layer, hidden layers, and output layer (Figure 3). In the inverse model, the input layer of neural network structure consists of input nodes where the input values comprise the volume per unit area of each grain size class at the spatial grids. Thus, the number of input nodes can be expressed as $M \times N$ where M and N are the total number of spatial grids and grain size classes, respectively. In this study, the number of dense hidden layers was set as three along with the total 2500 nodes, and thus total number of layers was five (Figure 3). Here, the rectified linear activation function (ReLU) was used as an activation function that calculates the output value from the total net weighted inputs (Ian & Yoshua, 2016). ReLU is function that is widely used for this purpose (Patterson & Gibson, 2017). The drop out has been applied to the hidden layer for regularization of the NN (Srivastava et al., 2014). The results of the feed-forward calculation of this NN during the training process were evaluated by the loss function (mean squared error), which is defined as follows:

$$J = \frac{1}{N} \sum \left(I_k^{fm} - I_k^{NN} \right)^2 \tag{10}$$

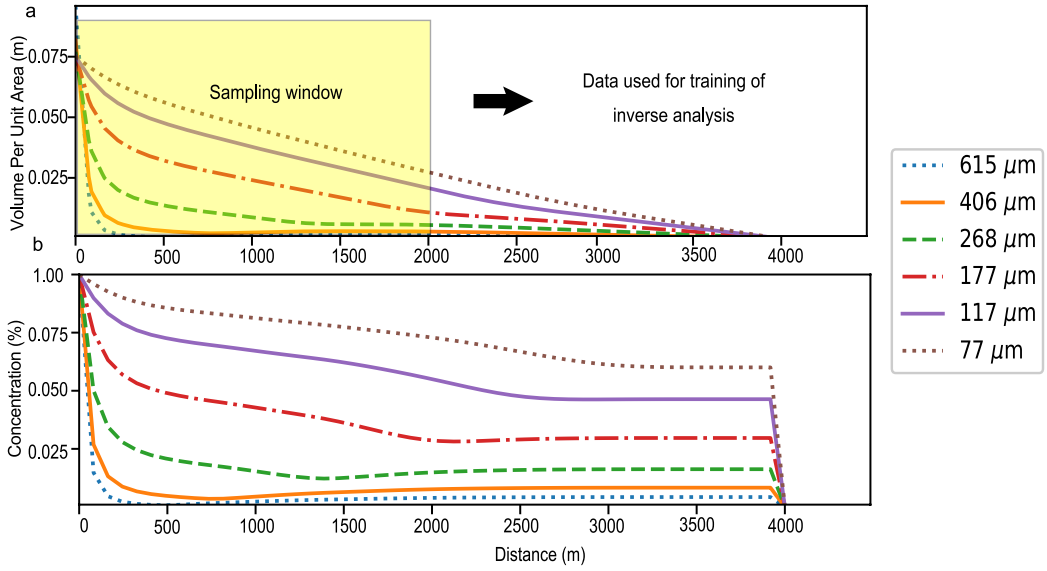

Figure 2. Example of the forward model calculation and sampling window used for the inverse analysis. (a) Spatial variation of the volume per unit area of each grain size class of the tsunami deposit calculated using the forward model. Here volume per unit area is used for exhibiting amounts of deposition of particular grain size class. Thickness of a tsunami deposit can be obtained by summation of volume-per-unit-area of all grain size classes with consideration of porosity. (b) Spatial variation of sediment concentration for each grain size class in the run-up flow when the tsunami reached maximum inundation point.

where I_k^{fm} is denoted as the teaching data that are the initial parameters used for producing in the training data and I_k^{NN} denotes the predicted parameters. This loss function quantifies how close the NN was to an ideal inverse model. The values of this function were averaged over the entire data set (Patterson & Gibson, 2017). To minimize the loss function J, the back-propagation method with the stochastic gradient descent algorithm (SGD) was used to optimize the weight coefficients at links of the network (Patterson & Gibson, 2017). The Nesterov momentum method was used with the SGD to speed up the computation and improve convergence (Sutskever et al., 2013). Although other optimizers such as AdaDelta, Adam, or AdaMax can provide an acceptable performance (Patterson & Gibson, 2017), this optimizer performed best for our model. This optimization process was repeated for prescribed times, and the training set was shuffled before splitting it into batch chunks that were used for the SGD optimization during each epoch.

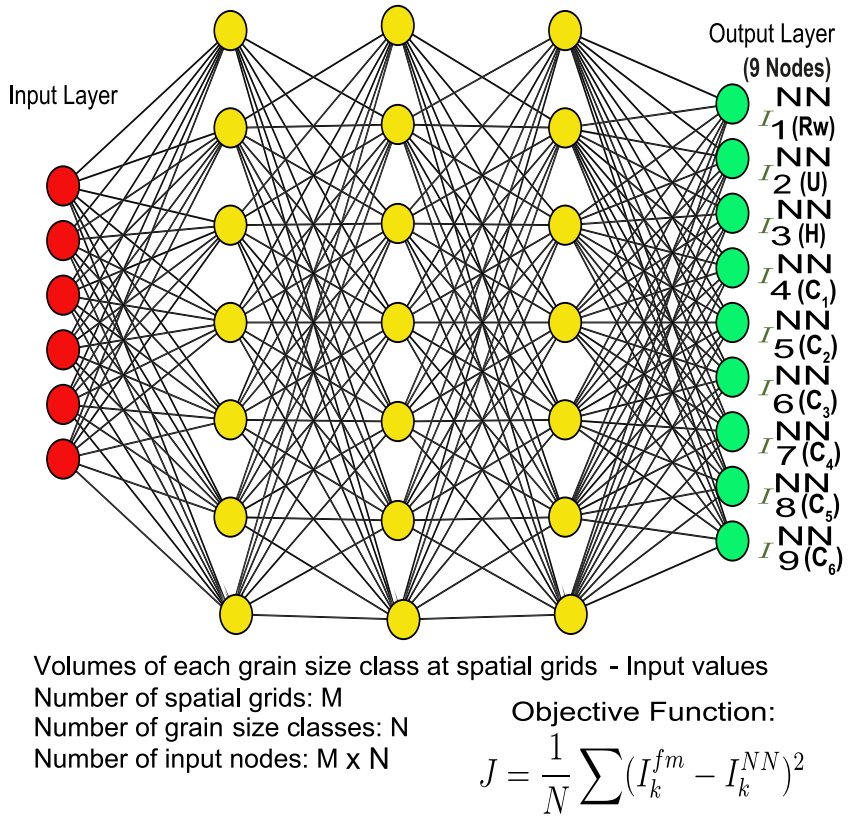

Figure 3. Neural network architecture for the inverse model. The NN structure includes one input and one output layer with three hidden layers for a total of five layers.

In order to estimate how well the model was trained without overfitting, validation was performed with the validation data set that was also generated from the forward model calculation. Among the produced data sets, 80% and 20% of the data were used for the training and validation respectively. The results of validation were used for tuning of the hyperparameters of the NN which are explained later. Finally, the performance of the model was evaluated after the hyperparameter tuning and using the test data sets, which were the data not used during the training process.

In our model, there are several hyperparameters that should be specified for the tuning of the training of the NN. The tuned hyperparameters were the learning rates, batch size and momentum used in the SGD, rates of drop out, number of hidden layers, types of activation function, and number of epochs. The hyperparameters were selected by trial and error in this study. The number of training data sets is also a hyper-

parameter of the inverse model, and it was tested by changing the number of repetitions of the forward model calculation. The trained model can work on a data set with a specific spatial grid in the fixed coordinate and grid spacing. In order to apply the inverse model to the natural data set in 1D vectors, the collected samples must be fit into that fixed coordinate system. A linear 1D interpolation was required as it provides values at positions between the data points, which are joined by straight line segments (Bourke, 1999). A linear 1D interpolation was applied to the natural data set in this case.

In addition to the training and validation data, 500 independent data points were kept aside for the testing of the inverse model. Therefore, after the model was trained, the model was applied to the test data sets to check its performance before applying it to the natural data sets. The good correlation between the teaching data in the test data set and the prediction of the model from the test data set showsfair ability of inverse model prediction. The residuals from the teaching data in the test data set were plotted in a histogram to determine the deviation of the prediction from the test data set from the true initial conditions.

3 Results of training and test of the inverse model

The hyperparameters for the training were set as follows. Among the hyperparameters (Table 1) used in the SGD algorithm, the learning rate was set as 0.02 and batch size was kept as 32 for our models (Patterson & Gibson, 2017). The use of larger or smaller learning rates did not provide improved results. Furthermore, other batch sizes were used in the training of the model, but the model was not improved. The selection of number of layers and the number nodes were tested by increasing or decreasing layers or nodes, and finally three hidden layers with 2500 nodes were used in the models. Another hyperparameter is the rate of drop-out at each hidden layer, which was 50% in our model. Thus, during the training, 50% of the layer outputs that were randomly selected were kept inactive. This regularization process helps to reduce overfitting and increases the efficiency of the training (Srivastava et al., 2014). Finally, the number of epochs in the training process, which indicates number of times that a full data set has passed the optimization calculation (J. Smith & Eli, 1995), were determined depending on the rates of the progress of the training (Figure 4). This is described in the following sections.

359 **Table 1.** List of hyperparameters used for major model configuration

Hyperparameter	Settings
Optimizer	SGD
Activation function	ReLU
Learning rate	0.02
Batch size	32
Momentum	0.9 (Nestrov)
Drop-out	50%
Number of epochs	2000
Number of hidden layers	3
Number of nodes	2500
Number of training data sets	4500

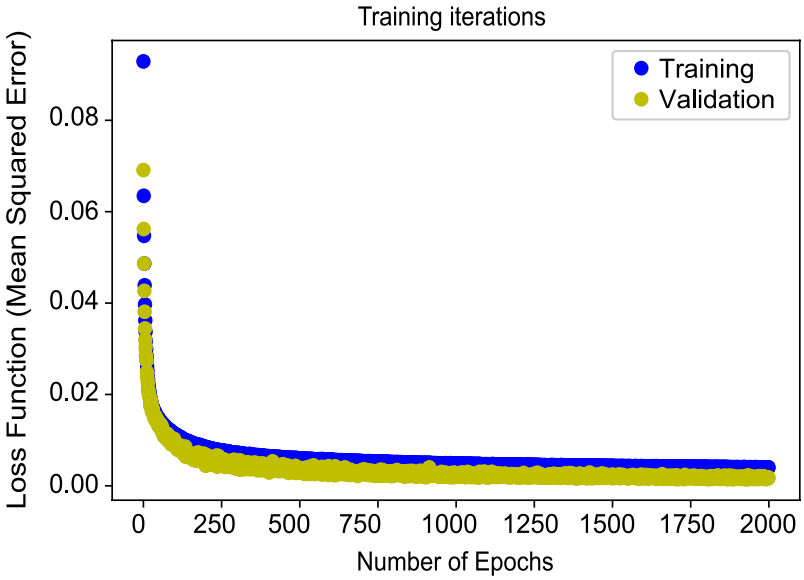

360 **Figure 4.** History of learning indicated by the variation of the loss function (mean squared
361 error). Both the values of the loss function for the training and validation data sets decrease over
362 2000 epochs without any discrepancy, thus indicating that overlearning did not occur.

363 The input parameters for the inverse model include the maximum inundation length,
364 flow velocity, maximum flow depth, and the sediment concentration of six grain size classes.
365 The range of values for the maximum inundation length, flow velocity, maximum flow

depth, and sediment concentration used for generating the training data sets were 2500 to 4500 m, 1.5 to 10 m/s, 1.5 to 12 m, and 0 to 2%, respectively. These ranges of flow conditions are also presumably applicable to other areas where large-scale tsunami inundated. These values are based on the maximum records of tsunamis in the studies of Mori et al. (2012), Nakajima and Koarai (2011), Foytong et al. (2013) and Jaffe et al. (2012).

The values of the loss function of training and validation at the first epoch were 0.09 and 0.07 for the training and validation data, respectively. The value of the loss function decreased to less than 0.01 after 200 epochs. The present model was reasonably converged over 2000 epochs for both the training and validation performance. Moreover, the plot for the loss function was smooth, and there was no anomalous oscillation. The last and lowest loss function at the final epoch was 0.0040 for the training data sets and was 0.0018 for the validation data sets. The efficiency of performance increases if the loss function reduces with the number of iteration or epochs with time. The aim is to achieve lowest value of loss function by tuning the hyperparameters in the neural network. The sampling window was set from 0 to 2000 m in this training and the following tests (Figure 2).

For the current inverse models, the forward model was calculated repeatedly from 500 to 4500 iterations, and it provided the best result with 4500 iterations of calculations of the forward model (Figure 5). Figure 5 presents a plot of the relation between the number of training data sets and the loss function of the validation data set. The loss value of the validation data set decreases as the amount of training data increases, which creates concave-upward shape. When the number of training data in the data set was 500, the loss function was higher but decreased significantly after 1500 training data sets. The loss function reached a minimum value after 3500 training data sets and did not change much subsequently. Thus, it was suggested that the number of training data sets should be greater than 3500. The number of training data sets thus used was 4500.

After training the model, the predictions of the inverse model estimates for test data sets were plotted against the original values used for producing the test data sets. Figure 6(a-i) shows that the nine predicted parameters from the artificial test data sets were distributed along the 1:1 line in the graph indicating that the test results were correlated with the original inputs.

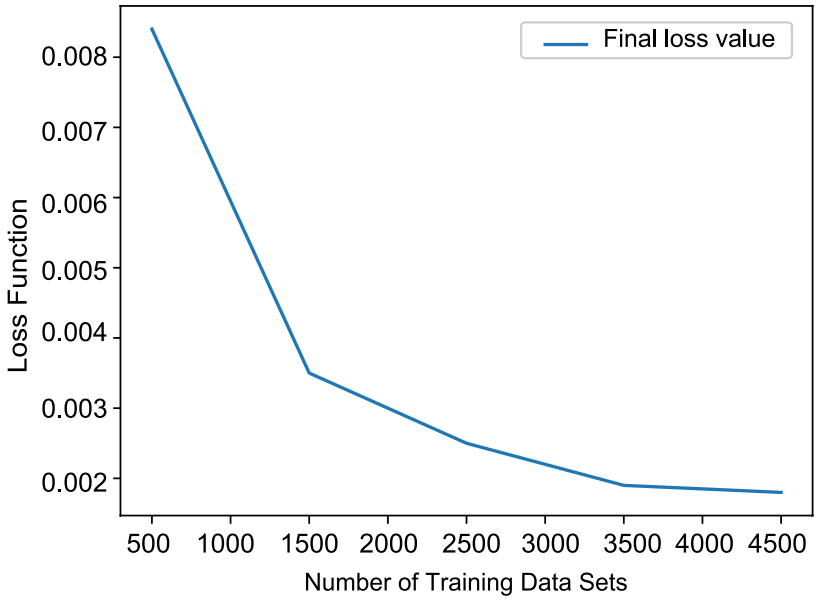

393 **Figure 5.** Relation between the loss function of the validation and number of training data
394 sets selected for the inverse model. The results of the training improved as the number of train-
395 ing data sets increased, whereas it varied slightly after 4000 training data sets.

405 Figure 7(a-i) shows histograms of the deviation of the estimated values predicted
406 from the original values. Deviations were distributed in a relatively narrow range with-
407 out large biases from the true conditions, except in the case of the maximum flow depth.
408 Only the maximum flow depth was slightly biased. Based on the scatter diagram (Fig-
409 ure 7), the values of the predicted maximum flow depth were approximately 0.5 m lower
410 than the input values.

413 4 Result of application to the 2011 Tohoku-Oki tsunami deposit

414 The model was applied to the 2011 Tohoku-Oki Tsunami deposits distributed around
415 the Sendai plain for the evaluation of the models. This region was extensively surveyed
416 for hazard evaluation as well as tsunami deposits (Abe et al., 2012; Naruse & Abe, 2017),
417 and thus, large amounts of field data are available for evaluating the inverse models. In
418 this study, the field data used was the same as that used for the FITTNUSS model (Naruse
419 & Abe, 2017), and therefore the inversion methodology can be compared with the pre-
420 vious study.

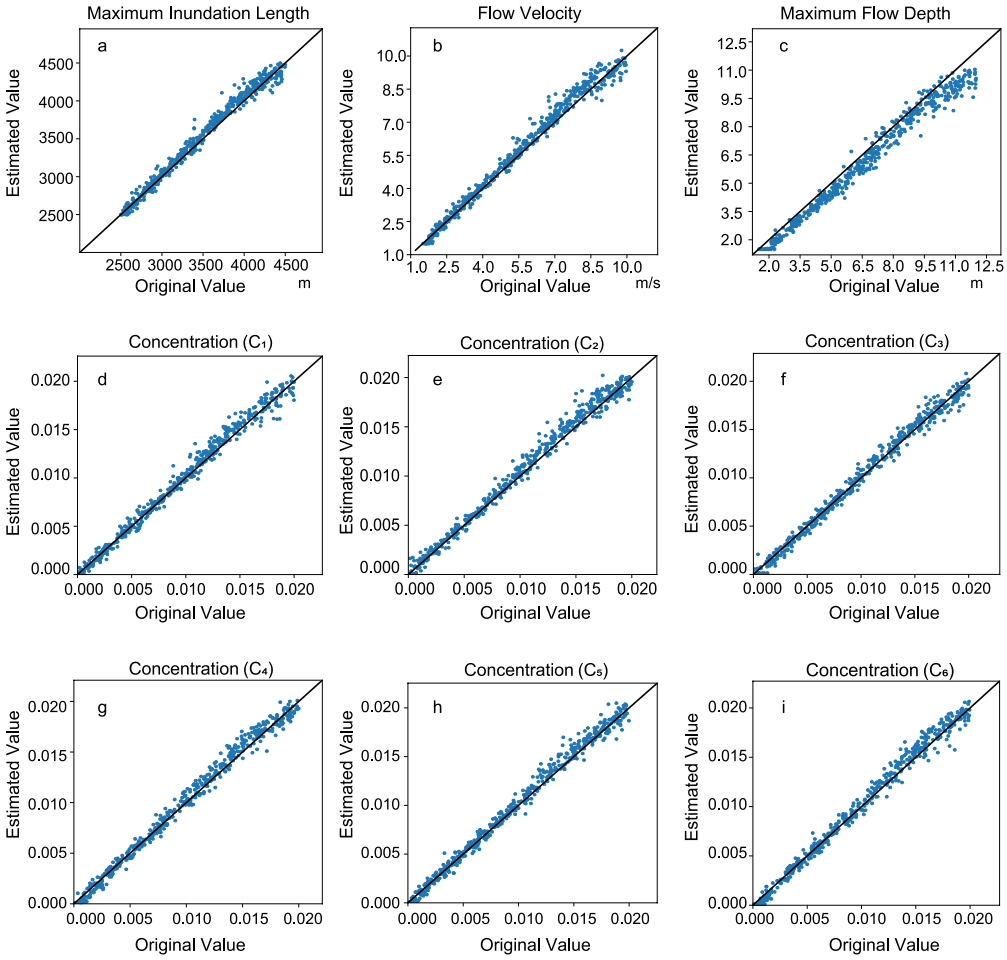

Figure 6. Verification of the performance of the model using artificial test data sets. The values estimated using the inverse model were plotted against the original values used for the production of the test data sets. The solid lines indicate a 1:1 relation and suggest good correlation.

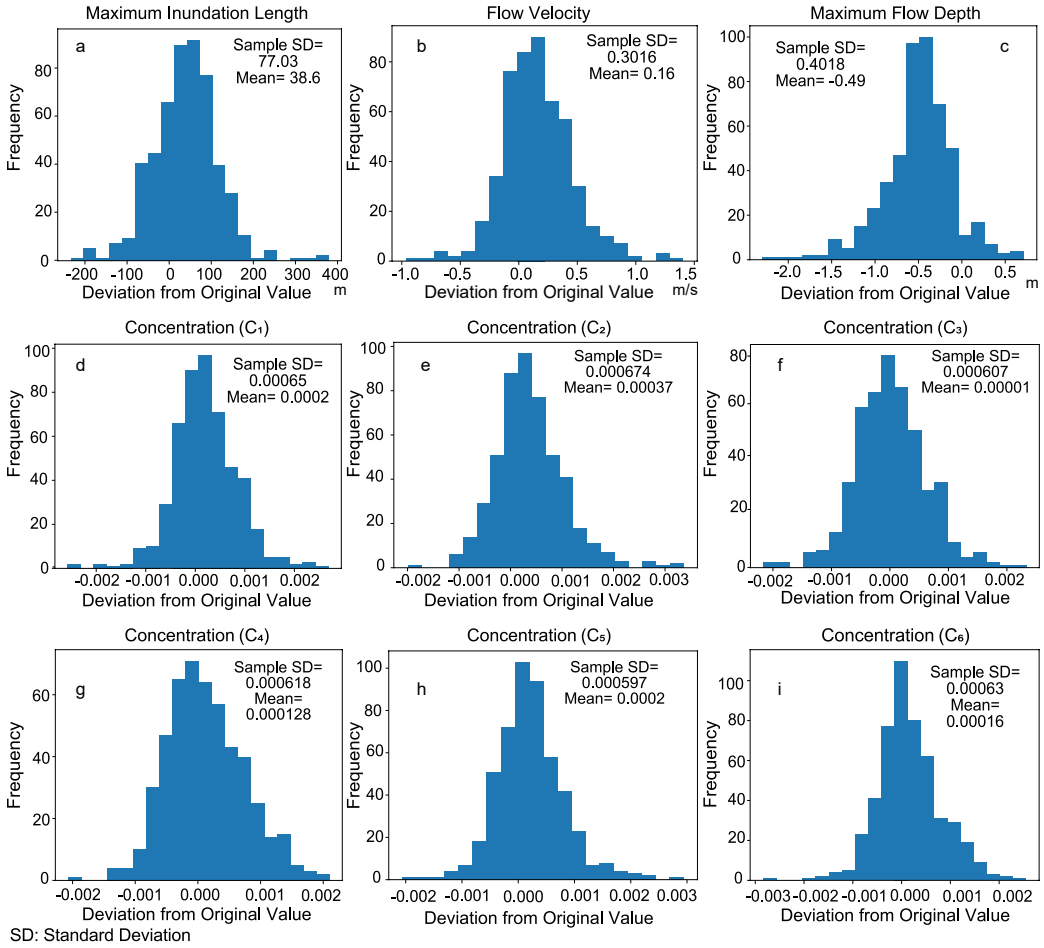

411 **Figure 7.** Histograms show the deviation of the predicted results from the original values of
412 the artificial test data sets.

4.1 Field methods and settings for inverse analysis

Field work for obtaining these tsunami deposits and collect auxiliary data was conducted soon after the tsunami event in June 2011 (Naruse & Abe, 2017).More detail on the methods are given in the studies of Abe et al. (2012) and Naruse and Abe (2017). The study area (Figure 8) mainly consists of a long sandy beach backed by a high onshore seawall, aeolian sand dunes, coastal forests, and long flat rice-paddy fields (Naruse & Abe, 2017). The deposit samples were obtained every 50–100 m at 26 sites along the transect. The thickness of tsunami sand and mud layers ranged from 0.1 cm to 34 cm. Grain size analysis of the tsunami deposit showed that the tsunami sand was primarily medium sand with a small amount of fine and very fine sand (Naruse & Abe, 2017). The measured grain size distributions were then discretized to six grain size classes (Figure 9), two more classes than used in the previous FITTNUSS model (Naruse & Abe, 2017). The representative diameters of the grain size classes were 615, 406, 286, 177, 117 and 77 μm .

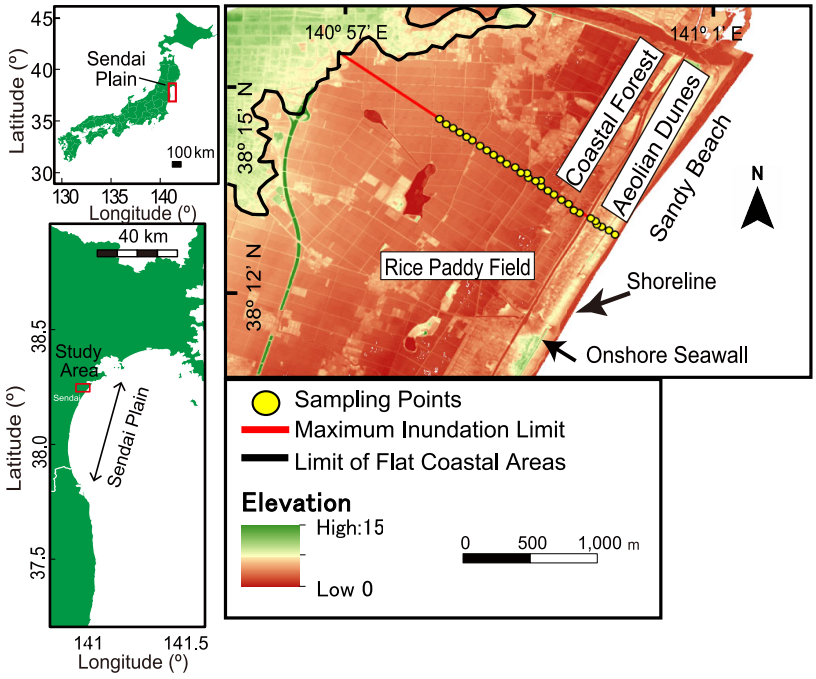

Figure 8. Location of the survey transect and sampling points on the Sendai plain. The location of the surveyed transect is shown on the topographic map of the study area. The 4 km long transect was situated transverse to the shoreline, and the tsunami deposit was sampled at 27 locations along the transect (Naruse & Abe, 2017).

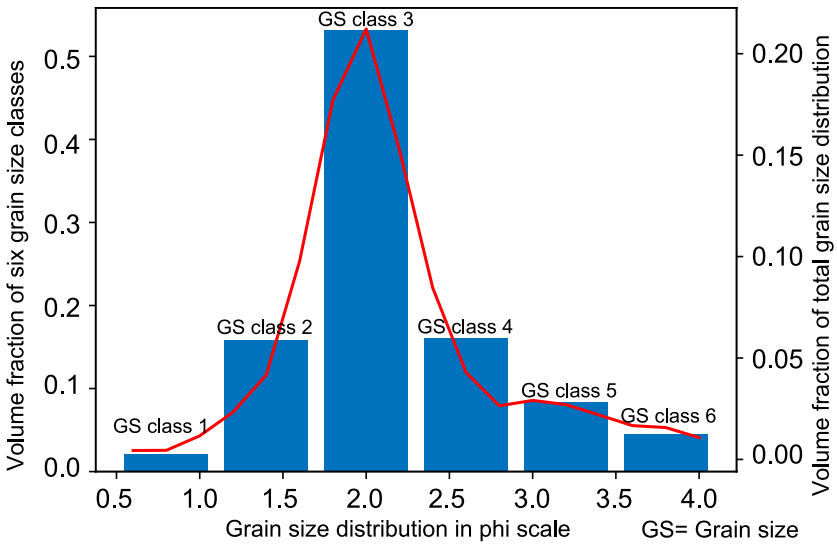

Figure 9. Total grain size distribution of the tsunami deposits in the Sendai plain and the discretized fraction of the sediments in the six grain size classes.

Parameters, such as flow velocity, estimated using the inverse model were verified by comparing them with the data obtained from aerial videos and observations of the Sendai plain (Hayashi & Koshimura, 2013; Mori et al., 2012). It is difficult to assess sediment concentration data obtained from direct field observation.

4.2 Determination of length of sampling window

The sampling window was set at a region from 0 to 2000 m along the transect. Although the total distance of the transect for collecting the samples was approximately 3000 m, the measured bed thickness was very thin (several millimeters) and exhibited a large fluctuation in the distal region (2000 to 3000 m) (Figure 13). Therefore, a 2000 m long sampling window was extracted from the sampling distance, which is 3000 m. This size of sampling window was also used for training the inverse model. For this situation, the number of spatial grids used for the inversion was 133 because the grid spacing in the fixed coordinates was 15 m. The selection of a sampling window of this size was checked based on a comparison with the results obtained using different sampling windows, and the results of the comparison suggested that 2000 m was the most suitable for obtaining stable results. Figure 11 shows the fluctuations of the jackknife standard error estimation of the parameters depending on the sampling window sizes. The equations re-

lated to jackknife standard error assessment are given in Appendix A. The majority of the parameters such as flow velocity and sediment concentrations exhibited a decreasing trend in their estimation errors as the length of the sampling window was increased. In particular, the jackknife error of the flow velocity decreased significantly above a sampling window size of 1000 m in length. The estimates of the maximum inundation length show large errors but it decreased suddenly at approximately 2500 m. In contrast, the error in the maximum flow depth increased above a sampling window size of 2000 m. Hence, it was decided that the size of the sampling window was set as 2000 m. It should be noted that the computation result for the maximum inundation length was unstable at this selection.

4.3 Effect of irregularly spaced data sets on the accuracy of the inversion

In field investigations, sampling intervals are larger than grid spacing of the artificial training and test data sets, and are irregularly spaced. Therefore, it is necessary to check the effect of non-ideal data sets such as incomplete field data sets on the results of inversion. In our model, 1D linear interpolation was applied to the field data set of Sendai plain to fit locations of data points to the spacing of training data sets, but this interpolation can have some influence on the predictions of the inversion model. Hence, after the model was trained, subsampling of test data sets was performed at the outcrop locations of Sendai plain. In this subsampling procedure, volume-per-unit-area of sediment in the test data sets at the sampling locations were estimated by 1D linear interpolation, and these subsampled data was subsequently interpolated again at the grids of the forward model. Therefore, the irregularly spaced data points were created from the original test data sets, and resulted in regularly spaced sampling locations due to repetition of 1D interpolation. The inverse analysis was conducted on this subsampled test data sets.

Finally, the model prediction was checked with both the true flow conditions and the inversion results using the original test data sets to examine the bias and variance caused by the incompleteness of spatial distribution of sampling locations. Figure 10a and 10b shows that the maximum inundation length and flow velocity have a bias towards positive end and mean of bias were 210 m and 0.50 m/s respectively. The maximum flow depth has negative bias 0.90 m (Figure 10c). Considering that it already had

506 **Table 2.** Predicted results by inverse model applied to 2011 Tohoku-Oki tsunami deposit data
507 obtained from Sendai plain

Parameters	Predicted Results	Mean bias
Maximum Inundation Length	4045 m ± 121.17 m	210 m
Flow Velocity	5.4 m/s ± 0.140 m/s	0.50 m/s
Maximum Flow Depth	4.11 m ± 0.152 m	-0.90 m
Concentration of C_1 (615 μm)	0.55% ± 0.034%	0.001
Concentration of C_2 (406 μm)	2.19% ± 0.048%	0.001
Concentration of C_3 (268 μm)	1.98% ± 0.058%	0.009
Concentration of C_4 (177 μm)	0.14% ± 0.018 %	0.009
Concentration of C_5 (117 μm)	0.18% ± 0.012%	0.001
Concentration of C_6 (77 μm)	0.04% ± 0.0011%	0.001

490 a bias of 0.50 m in the inversion results of the original test data sets, the additional bias
491 caused by incompleteness of data sets was 0.40 m towards negative end. Figure 10(d-
492 i) shows that the bias in sediment concentrations were generally around 0.001.

497 ### 4.4 Result of inversion

498 The inverse model reconstructed the flow conditions of the tsunami from the de-
499 posit of the 2011 Tohoku-Oki tsunami in the Sendai plain. The model estimated flow
500 parameters that were close to the observed values. The maximum inland extent of tsunami
501 deposits observed by Mori et al. (2012), was up to 4.02 km beyond the shoreline and the
502 tsunami had inundation height of 6.5 m above Tokyo Peil (mean sea level at Tokyo bay),
503 which transported large amount of sandy sediments landward (Mori et al., 2012). The
504 average flow velocity of the run-up flow was measured 4.2 m/s from an aerial video which
505 varied landward from 6.9 to 1.9 m/s (Hayashi & Koshimura, 2013).

508 Table 2 shows the predicted hydraulic conditions of the 2011 Tohoku-Oki tsunami
509 of the Sendai plain. The predicted result of the flow velocity was approximately 5.4 m/s
510 with a range of uncertainty ± 0.140 m/s using jackknife standard error calculation with
511 a 95% confidence interval (Figure 12b). The value of the maximum flow depth was ap-

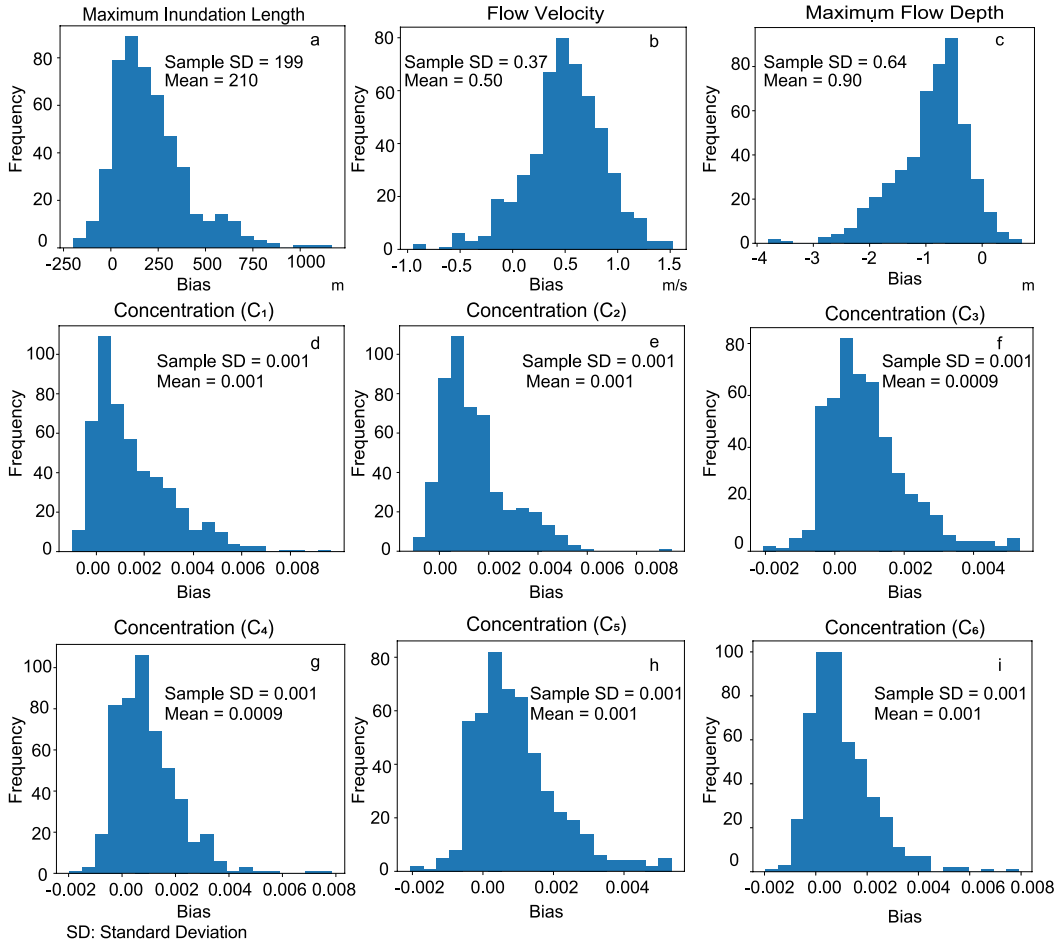

493 **Figure 10.** Histograms showing the variance and bias of predictions from the test data sets
494 subsampled at the sampling locations in Sendai plain.

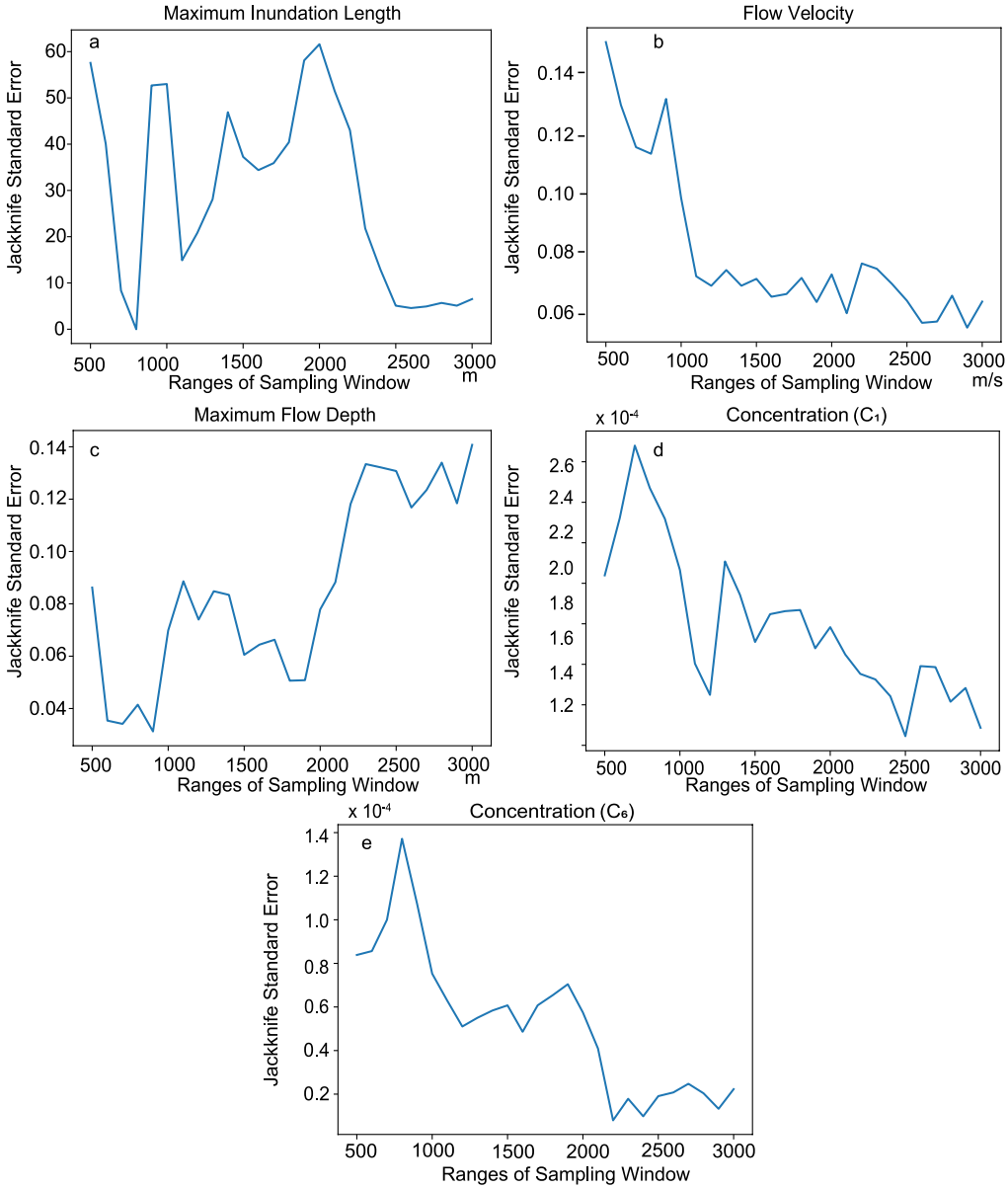

Figure 11. Variation of jackknife standard error with changing range of sampling window distance.

poximately 4.11 m (± 0.152 m uncertainty using jackknife standard error calculation (Figure 12c) with a 95% confidence interval).

The reconstructed total sediment concentration over six grain size classes was 5.08%. The estimated value of the sediment concentration of each grain size class ranged from 0.04% to 2.19% (Figure 12d-12i).

The model predicted the maximum inundation length of the tsunami from the deposit, as approximately 4045 m with a ± 121.17 m jackknife standard error with a 95% confidence interval (Figure 12a). The actual inundation length was 4020 m (Naruse & Abe, 2017), which is consistent with the reconstructed value. Table 2 also shows, mean bias which are the mean of the bias estimates for 9 parameters, caused large and irregular spacing of the sampling points. The maximum inundation length shows 210 m bias and flow velocity shows 0.50 m/s bias towards positive end, whereas the maximum flow depth shows total 0.90 m bias towards negative end. Bias in the sediment concentration was around 0.001.

Finally, using the reconstructed initial conditions of the tsunami, the forward model was used to calculate the spatial distribution of the thickness and grain size composition for a comparison with the measured distribution. Figure 13 exhibits the thickness and grain size distribution with the distance for the measured data and simulated results. The measured values of volume per unit area for each grain size class matched the simulated results except in the case of the finest grain size class, where the predicted values were larger than the actual measurements.

5 Discussion

5.1 Tests of inverse models

The tests of the inverse models performed using the artificial data sets of tsunami deposits demonstrated that the models built using NN can predict the flow velocity and the concentration of six grain size classes, maximum inundation length reasonably. The scatter diagram of the predicted parameters against the true conditions indicates excellent correlation (Figure 6). For example, 2σ of the estimation error of the maximum inundation length was 121.17 m, and the range of true values was 2500–4500 m (Figure 12). Thus, the precision of estimates is only the order of approximately 5%. More importantly, there was no large deviation of mode of predicted values from true conditions

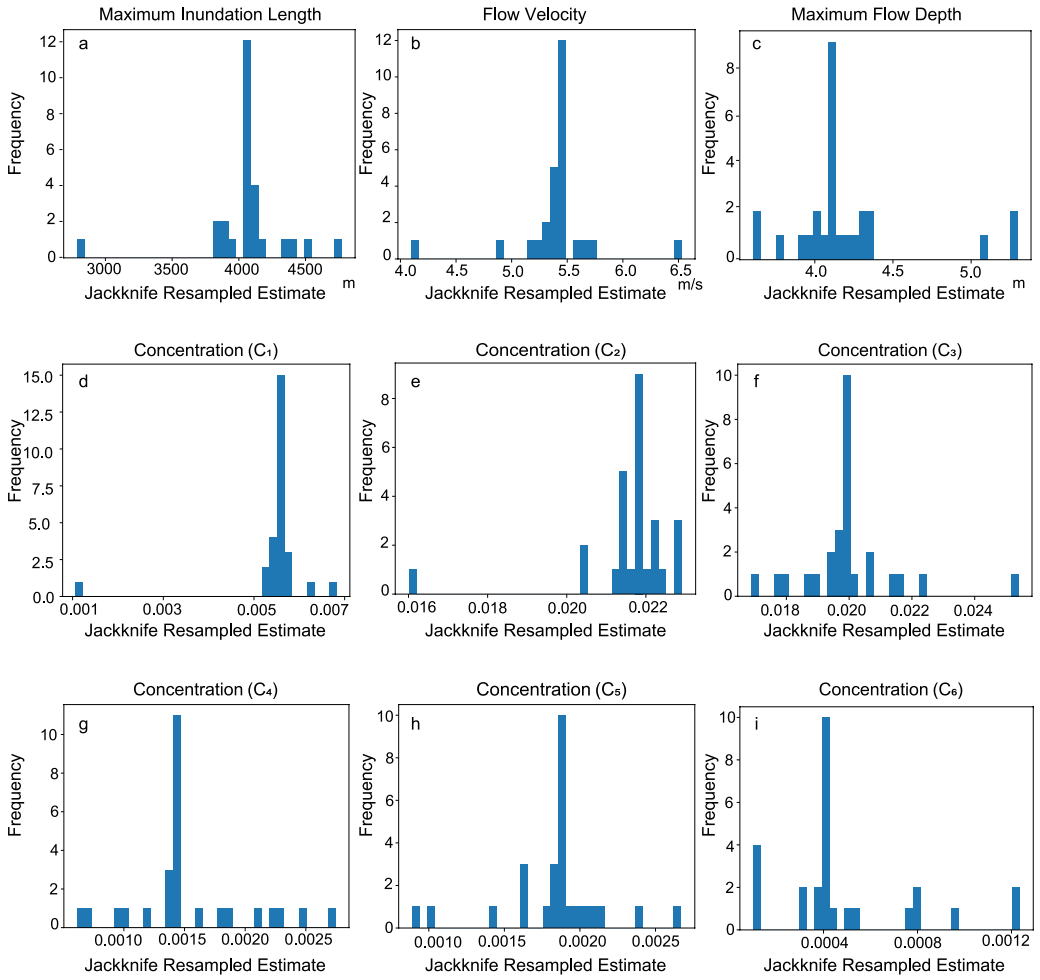

Figure 12. Jackknife estimates for the results predicted by the inverse model to determine the uncertainty of the model.

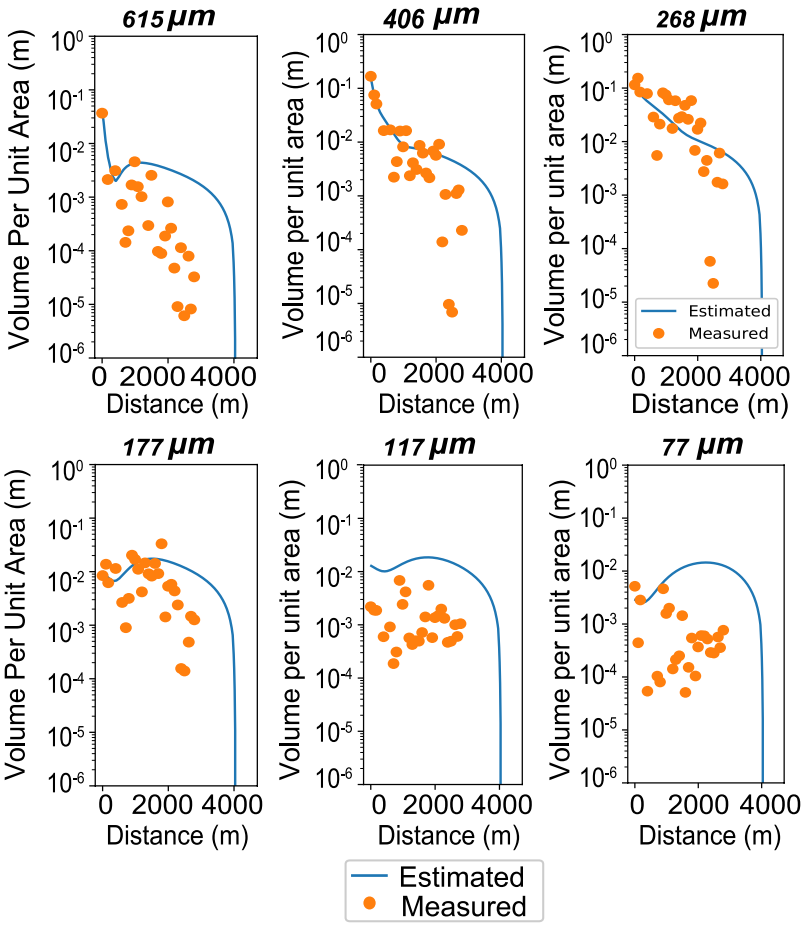

528 **Figure 13.** Spatial variation of the thickness of the tsunami deposit. Spatial distribution of
529 volumes per unit area of six grain size classes is presented. The solid circles indicate the values
530 measured by Naruse and Abe (2017), and the lines indicate the results of the forward model
531 calculation obtained using parameters predicted by the inverse model.

555 except for the maximum flow depth. Especially in cases of estimates of sediment con-
556 centration, mean of the estimation errors ranges within 1.0×10^{-3}. These results im-
557 ply that the inverse model has the ability to possess the prediction of hydraulic condi-
558 tions satisfactorily.

559 However, the model tends to estimate maximum flow depth values that are approx-
560 imately 0.5 m higher. As a result, in the comparison of the predicted values and orig-
561 inal values of the maximum flow depth plotted in the histogram, the deviation shows a
562 positive bias, and the mode value was approximately 0.5 m towards the negative side.

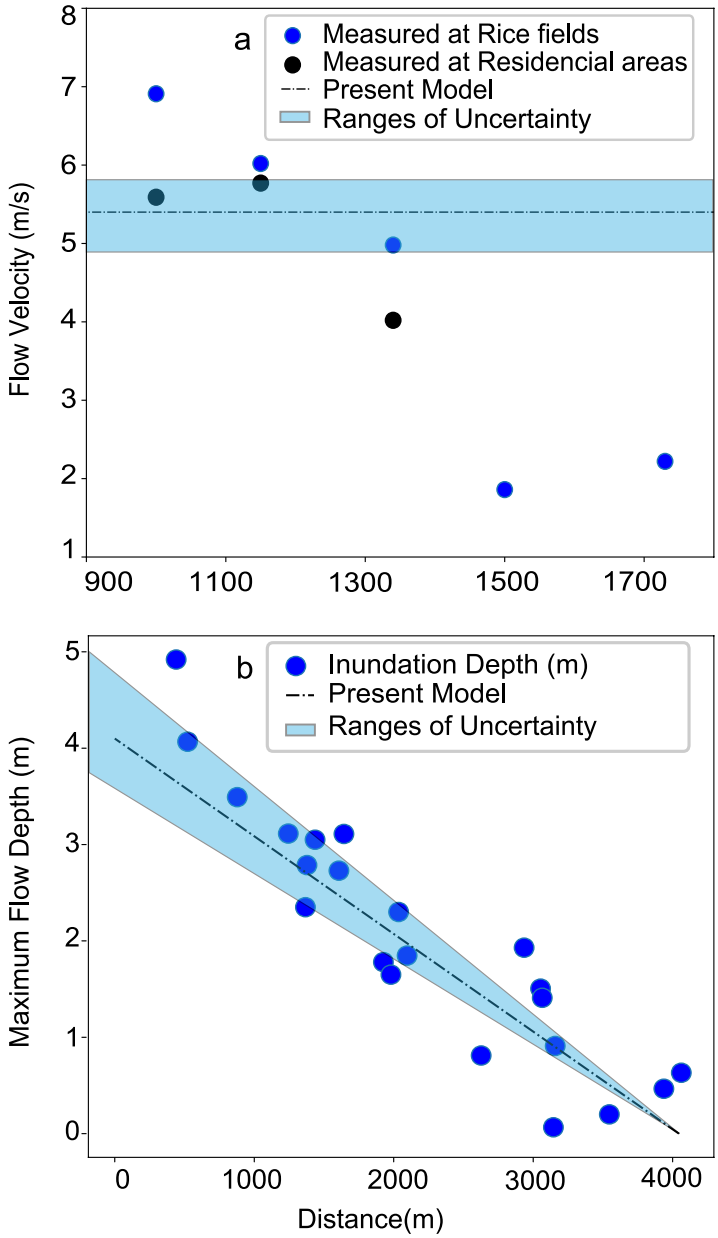

532 **Figure 14.** Comparison between field observation and results of inverse analysis of 2011
533 Tohoku-Oki tsunami. The solid dots are measured values by field observation, and the lines are
534 results of the inverse analysis of this study. (a) Velocity of run-up flow of the 2011 Tohoku-Oki
535 tsunami on Sendai plain. (b) Maximum flow depth of 2011 Tohoku-Oki tsunami on Sendai plain.
536 Values measured from the aerial videos are indicated by the solid and open circles (Hayashi &
537 Koshimura, 2013), and the results of the inverse analysis are shown by the lines.

Despite the skewness, it is possible to correct the final result of the maximum flow depth by adding 0.5 m with the final reconstructed value from original field data.

5.2 Reconstruction of the flow parameters of the 2011 Tohoku-Oki tsunami

After applying the inverse models to the 2011 Tohoku-Oki tsunami, the predicted results of the flow velocity and the inundation depth were close to the values observed in the aerial video and field measurements (Figure 14), which indicates the effectiveness of the proposed method in applying the actual tsunami deposits.

The subsampling test showed (Figure 10) that the inversion model has slight bias for maximum inundation length, flow velocity and the maximum flow depth because of the effect of large and irregular interval of sampling locations. The flow velocity shows 0.50 m/s mean bias towards the positive end. Therefore, the predicted value of flow velocity 5.4 m/s could be approximately 4.9 m/s considering the bias correction. Figure 14 shows that the observed inundating flow velocity of 2011 Tohoku-Oki tsunami measured by video records varies spatially from 1.9 to 6.9 m/s (Hayashi & Koshimura, 2013), and the reconstructed values and the reconstructed values along with the jackknife uncertainty estimates (4.8–5.8 m/s) are in the range of observed values.

The predicted inundation length was 4045 m which is close to the original maximum inundation length of approximately 4020 m. However, the mean bias for this parameter caused by incompleteness of field data sets was 210 m (Figure 10; Table 2). Hence, the bias corrected reconstructed values of the maximum inundation length could be approximately 3835 m which is still close to the maximum inundation length measured in the field (Naruse & Abe, 2017). Furthermore, the model predicted the concentration of six grain size classes satisfactorily. The range of the estimated concentration for each grain size class was 0.04–2.19 vol.%, and the total concentration was 5.08 vol.%. There has been no direct observation of the sediment concentration in the inundating tsunami flows, and thus, it is impossible to compare the reconstruction with the actual observation.

The predicted results for the maximum flow depth were close to the observed maximum flow depth in the field data (Figure 14). The model predicted 4.11 m that approximates the observed values well. The uncertainty analysis performed using the jackknife method indicated that the error of estimates for maximum flow depth ranges from 3.8 m to 4.4 m, which is reasonably narrow for an assessment of the magnitude of the tsunami.

However, considering the total mean bias caused by both original and interpolation of the field data sets, 0.90 m should be added to the maximum flow depth predicted by the inverse model (Figure 14). Thus, the reconstructed value obtained can be corrected to 5.0 m, which is closer to the observed data set.

This is to be noted that the effect of the friction coefficient (C_f) on the results of inversion was investigated to check forward model influence on the inversion results. Estimates of flow velocity varied from 5.5 to 3.08 m/s in response to the variation of C_f from 0.002 to 0.01. The present study uses C_f value 0.004 as the same was used in the FITTNUSS model (Naruse & Abe, 2017). The variation of reconstructed values of inundation depth varied only from 4.8 to 5.0 m and sediment concentration in response to varied C_f was negligible. To summarize, the result obtained using a largest value of friction coefficient (C_f) corresponds to the higher velocity in inversion results, but other flow characteristics were not influenced largely. Therefore, it is important to specify realistic friction coefficient value in the forward model to estimate flow velocity. The influence of number of grain size classes on the inversion results was also checked. The variation of the results was negligible for all reconstructed values (see supplementary information). Hence, the assumptions in the forward model have least influence on the inversion results.

5.3 Comparison with existing models

In the present study, we presented the use of a deep-learning NN as an inversion technique with a modified FITTNUSS forward model to obtain the initial tsunami hydraulic condition based on tsunami deposits. The advantages of this new methodology are that (1) it can employ a more realistic forward model than previous methods, and (2) the performance of the inverse model can be tested before its application to actual deposits by using artificial data sets. In addition, (3) it is possible to conduct an uncertainty analysis of the inversion using the resampling method owing to the computational efficiency of the model. However, the data set of 2011 Tohoku-Oki tsunami deposits in Sendai plain is one of the best records of tsunami deposits in history. The data set contains high resolution samples as well as observational records of flow velocity and flow depth. However, further verification of the methodology using other case studies is strongly needed in future studies for proving wide applicability of the method.

Firstly, the DNN inverse model can employ the forward model, which is computationally expensive. The new inverse model requires only a limited number of iterations of the forward model calculation for producing the training data sets, and these iterations can be parallelized. The calculation for producing each training data set is independent. In contrast, the previous inverse models, including the FITTNUSS model (Naruse & Abe, 2017), employed the optimization method (e.g., LBFGS) in which the forward model calculation depends on the result of the previous iteration, and thus, this trial and error procedure cannot be parallelized. It was time consuming to obtain the best solution and was difficult to improve the computational efficiency in the previous methodology. Therefore, the previous inverse model only employed the largely abridged forward models such as the "moving-settling tube" (Soulsby et al., 2007) or sudden settling from equilibrium uniform flows (Jaffe & Gelfenbuam, 2007). The recent inverse model TSUFLIND (Tang et al., 2018; Tang & Weiss, 2015) also probably employed a similar simplified assumption because of this computational load problem. Tang et al. (2018) proposed the inversion model with uncertainty analysis using TSUFLIND-EnKF method but this method shares the same limitations of TSUFLIND in the assumption of the forward model. In addition, optimization by EnKF requires iteration of calculation that cannot be parallelized, while production of training data sets in our method can be easily parallelized so that it can employ computationally expensive models (Tang et al., 2018).

In the new inverse model, this limitation is diminished in the forward model, such that the former can potentially employ fully hydrodynamic models as the forward model. The present method of DNN is relatively robust against the sampling measurement errors as the uncertainty can be evaluated by jackknife method which was not applied to any other inverse models. Furthermore, forward model can be easily replaced with the similar or other upgraded forward models to improve our inverse model. This phenomenon implies that the present inverse model is flexible for upgradations.

Secondly, the inverse model proposed herein can be tested prior to the actual analysis because each inversion (i.e., feed-forward calculation of the NN) is completed instantaneously in this method. In previous methods, such as FITTNUSS, each inversion requires a long time such that it was not realistic to iterate the inversion several hundred times for testing the performance of the model. In addition, a modern statistical uncertainty analysis requires resampling procedures in which the iteration of the inversion is also required. Therefore, it was possible to apply the jackknife uncertainty analysis in

the case of the DNN inversion in this study, but it is difficult to provide an error range of the estimates for the FITTNUSS method or other methods in a realistic time period.

The inverse model in this study uses inexpensive artificial data for training of the neural network to avoid the difficulties to gather large amounts of data sets of tsunami deposits with in-situ measurements of flow velocity and depth. Even if the measured values of tsunami characteristics are available, the overfitting of the inverse model should not be avoided because number of those data sets must be limited. The random generation of artificial training data sets for different parameters was adopted to bypass the drawbacks of using real measurements to train the inverse model (Le et al., 2017; Tobin et al., 2017; Tremblay et al., 2018). Bias due to inaccuracy of the forward model may occur in this methodology as all of other inverse models, and thus it is necessary for accurate reconstruction to seek the forward model based on the appropriate assumptions for the field. As described above, the framework of inversion employed in this study is flexible to adopt a realistic forward model.

6 Limitation and scope of improvement

The present model shows promising results, but the reliability of this model is required to be validated by using more field data. The options and hyperparameters of the inversion, such as the sampling window size, can be tested using other examples of modern tsunami deposits with known flow parameters. Furthermore, it is necessary to apply this model to tsunami deposits in Tohoku and other regions along with older tsunami deposits in order to scrutinize the present model comprehensively and to develop a robust model that can be used in the relevance of hazard evaluation.

In addition, the model still has some limitations in terms of its applicability and accuracy. For example, the reconstructed values of the maximum flow depth showed a bias of -0.5 m, and the additional bias caused by the effect of irregularly spaced data sets on the inversion results. In future studies, improving the algorithm of the neural network structure might eliminate or reduce the bias of the parameter. Notwithstanding the bias in the predicted values of the parameters such as, maximum inundation length, flow velocity, maximum flow depth, this model showed satisfactory results for tsunamis of any scale. Our model is not suitable for the regions with topographic lows and channels along with the high slope areas where return flow is strong. The assumption of quasi-

steady run-up flow analysis will only work in regions where the topography is sufficiently smooth and slope can be regarded as constant. Also, the forward model assumptions are valid only at depositional areas. Thus, a coastal dike or problems in source areas are not necessary to consider (Naruse & Abe, 2017), and therefore the erosional areas must be excluded in the inverse analysis using our method. These simplifications are adequate for the Sendai plain as suggested by verification of our inversion result. In future studies, it is needed for verify influence of degree of topography on the inversion results, and other forward models will be tested if necessary. The improvement of the model can be done by incorporating 2D shallow-water model in future.

It is to be noted that, in the present study thickness of the deposit for one run-up flow or layer is considered. Thus, in case of deposits that exhibit multiple layers (Abe et al., 2020), one of layers must be chosen for the analysis. Hence, if a single layer cannot be traced in a region, it is impossible to apply our model to that region. Since, the 2011 Tohoku-Oki tsunami deposits on Sendai plain were mostly observed as single sand layer formed by the first wave, it was possible to apply our model to Sendai plain (Abe et al., 2012).

7 Conclusion

The new model presented in this study uses an artificial NN to derive the hydraulic conditions of a tsunami. It successfully reconstructed the flow conditions including the maximum inundation length, flow velocity, maximum flow depth and sediment concentrations from artificial tsunami deposits produced by the forward model as well as the natural tsunami deposits of 2011 Tohoku-Oki tsunami. The reconstructed flow velocity and maximum depth were 5.4 m/s and 4.11 m respectively, which are in the ranges of observed values of the tsunami. The uncertainty of the results was determined using the jackknife method, which also shows that the model yields results that do not comprise large ranges of data. Thus, in future studies, it is expected that this model would be able to successfully reconstruct the flow conditions of modern and ancient tsunamis.

Notation

The symbols L, M and T denote dimensions of length, mass and time respectively. The symbol [1] denotes that the value is dimensionless.

719 $\boldsymbol{C}$ Total layer-averaged sediment concentration [1]

720 $\boldsymbol{C_i}$ Layer-averaged sediment concentration of the ith grain size class [1]

721 $\boldsymbol{C_f}$ Bed friction coefficient [1]

722 $\boldsymbol{E_{si}}$ Sediment entrainment coefficient [1]

723 $\boldsymbol{F_i}$ Volumetric fraction of the ith grain size class in the active layer [1]

724 $\boldsymbol{H}$ Maximum flow depth of the tsunami at the seaward (upstream) boundary of the tran-
725 sect [L]

726 $\boldsymbol{L_a}$ Thickness of the active layer [L]

727 $\boldsymbol{R_w}$ Maximum inundation length [L]

728 $\boldsymbol{S}$ Bed slope [1]

729 $\boldsymbol{U}$ Run-up velocity of the tsunami [LT^{-1}]

730 $\boldsymbol{g}$ Acceleration of gravity [LT^{-2}]

731 $\boldsymbol{h}$ Flow depth of the tsunami [L]

732 $\boldsymbol{r_{0i}}$ Ratio of near-bed sediment concentration of the ith grain size class to layer-averaged
733 concentration [1]

734 $\boldsymbol{t}$ Time [T]

735 $\boldsymbol{u_*}$ Friction velocity [LT^{-1}]

736 $\boldsymbol{w_{si}}$ Settling velocity of sediment of the ith grain size class [LT^{-1}]

737 $\boldsymbol{x}$ Bed-attached streamwise coordinate [L]

738 $\boldsymbol{\eta_i}$ Volume per unit area of sediment of the ith grain size class [L]

739 $\boldsymbol{\lambda_p}$ Porosity of the tsunami deposit [1]

740 $\boldsymbol{\mu}$ Dimensionless settling velocity of sediment of the ith grain size class [LT^{-1}]

741 $\boldsymbol{\tau_{*m}}$ Shields dimensionless shear stress using the mean grain size in the active layer [1]

742 $\boldsymbol{\psi_i}$ Coefficient in the relation of turbulent suppression due to density stratification [1]

743 $\boldsymbol{X_{norm}}$ Normalized values of input data [1]

744 $\boldsymbol{X_{raw}}$ Original values of the input data respectively [1]

745 $\mathbf{min}(\boldsymbol{X_{raw}})$ Minimum values of the raw input data [1]

746 $\mathbf{max}(\boldsymbol{X_{raw}})$ Maximum values of the raw input data [1]

747 $\boldsymbol{Y_{norm}}$ Normalized values of teaching data [1]

748 $\boldsymbol{Y_{raw}}$ Original values of the teaching data respectively [1]

749 $\mathbf{min}(\boldsymbol{Y_{raw}})$ Minimum values of raw teaching data [1]

750 $\mathbf{max}(\boldsymbol{Y_{raw}})$ Maximum values of raw teaching data [1]

751 $\boldsymbol{I_k^{fm}}$ Teaching data that are the initial parameters used for producing in the training
752 data
753 $\boldsymbol{I_k^{NN}}$ Predicted parameters using Neural networks
754 $\boldsymbol{J}$ Loss function for the inverse model

755 **Acknowledgments**

756 The source codes and all other data of DNN inverse model are available in Zen-
757 odo (`http://doi.org/10.5281/zenodo.3881964`), which is the open access data repos-
758 itory. We express our sincere gratitude to Prof. Takao Ubukata and other researchers
759 in the biosphere study group of Kyoto University for their valuable suggestions. We thank
760 Sediment Dynamics Research Consortium (sponsored by INPEX, JOGMEC, JX Nip-
761 pon Oil & Gas Exploration Corporation, JAPEX) for funding. The authors thank Ky-
762 oto University for providing access to the required facilities and the Ministry of Educa-
763 tion, Culture, Sports, Science and Technology, Japan, for providing the permission and
764 scholarship for conducting this collaborative research in Japan. We are thankful to the
765 editor Amy East, Bruce Jaffe and two anonymous reviewers for their detailed and con-
766 structive reviews that greatly improved the paper.

767 Appendix A Uncertainty analysis of inversion results

768 The jackknife method was used for the error assessment of the results of the inverse
769 model. This method estimates the standard error of the predicted value of the model
770 using a resampled population. Quenouille (1949) first introduced this resampling method
771 (Nisbet et al., 2009).

772 A jackknife test is similar to the bootstrap method, but instead of a random sam-
773 pling of a data set, the inversion model works on each separate set of samples by omit-
774 ting a single set of observations per iterations from a total of N observations. Inversions
775 are carried out N times and the resulting ensemble of solutions were interrogated to a
776 single estimate for each parameter. In short, it involves a leave-one-out strategy in a data
777 set of N observations and the model works on the rest of the samples and gives results
778 accordingly. Preferably, $N-1$ observations were built on the data set as resampled data

for the model. Farrell and Singh (2010) discussed the importance of the jackknife method in survey sampling.

We briefly describe the jackknife uncertainty analysis. Sample and jackknife estimates are denoted as S and S^*, respectively. The number of observations in the sample is N and the set of observations is denoted as $\{X_1, ..., X_n, ..., X_N\}$. The sample estimate of the parameter is a function of the observations in the sample (Abdi & Williams, 2010). The equation is given as follows:

$$S = f(X_1, ..., X_n, ..., X_N) \tag{A1}$$

Let S_{-n} be the $n-$th partial prediction of the parameter, which is produced by the inverse model without the nth observation. The equation for the prediction S_{-n} is given as follows:

$$S_{-n} = f(X_1, ..., X_{n-1}, X_{n+1}..., X_N) \tag{A2}$$

S_n^* represents a pseudo value estimation of the nth observation. This parameter is defined as the difference between the estimates S obtained from the entire sample and the estimates S_{-n} obtained without the nth observation as follows:

$$S_n^* = NS - (N-1)S_{-n} \tag{A3}$$

The mean of the pseudo values are regarded as the jackknife estimate S^*. The equation for the jackknife estimate is given as follows:

$$S^* = S_{mean}^* = \frac{1}{N}\sum_{n}^{N} S_n^* \tag{A4}$$

where S_{mean}^* is also the mean of the pseudo values. The variance of the pseudo values is denoted as σ_{JK}^{var} and the formula for the variance is given as follows:

$$\sigma_{JK}^{var} = \frac{\sum(S_n^* - S_{mean}^*)^2}{N-1} \tag{A5}$$

Finally, the jackknife standard error of the parameter estimate is denoted as σ_{JK}^{SE}, The formula for the jackknife standard error is

$$\sigma_{JK}^{SE} = \sqrt{\frac{\sigma_{JK}^{var}}{N}} = \sqrt{\frac{\sum(S_n^* - S_{mean}^*)^2}{N(N-1)}} \tag{A6}$$

The confidence interval for this study has been computed using this jackknife standard error formula.

References

Abdi, H., & Williams, L. J. (2010). Jackknife. *Encyclopedia of research design*, *2*.

Abe, T., Goto, K., & Sugawara, D. (2012). Relationship between the maximum extent of tsunami sand and the inundation limit of the 2011 tohoku-oki tsunami on the sendai plain, japan. *Sedimentary Geology*, *282*, 142–150.

Abe, T., Goto, K., & Sugawara, D. (2020). Spatial distribution and sources of tsunami deposits in a narrow valley setting-insight from 2011 tohoku-oki tsunami deposits in northeastern japan. *Progress in Earth and Planetary Science*, *7*(1), 1–21.

Bishop, C. M., et al. (1995). *Neural networks for pattern recognition*. Oxford university press.

Bourgeois, J., Bernard, E., & Robinson, A. (2009). Geologic effects and records of tsunamis. *The sea*, *15*, 53–91.

Bourke, P. (1999). Interpolation methods. *Miscellaneous: projection, modelling, rendering.*(1).

Braaten, D., Shaw, R., et al. (1990). Particle resuspension in a turbulent boundary layer-observed and modeled. *Journal of Aerosol Science*, *21*(5), 613–628.

Choowong, M., Murakoshi, N., Hisada, K.-i., Charusiri, P., Charoentitirat, T., Chutakositkanon, V., ... Phantuwongraj, S. (2008). 2004 indian ocean tsunami inflow and outflow at phuket, thailand. *Marine Geology*, *248*(3-4), 179–192.

Costa, P. J., Andrade, C., Cascalho, J., Dawson, A. G., Freitas, M. C., Paris, R., & Dawson, S. (2015). Onshore tsunami sediment transport mechanisms inferred from heavy mineral assemblages. *The Holocene*, *25*(5), 795–809.

Crank, J. (1984). *Free and moving boundary problems*. Clarendon press Oxford.

Dietrich, W. E. (1982). Settling velocity of natural particles. *Water resources research*, *18*(6), 1615–1626.

Farrell, P. J., & Singh, S. (2010). Some contributions to jackknifing two-phase sampling estimators. *Survey Methodology*, *36*(1), 57–68.

Foytong, P., Ruangrassamee, A., Shoji, G., Hiraki, Y., & Ezura, Y. (2013). Analysis of tsunami flow velocities during the march 2011 tohoku, japan, tsunami. *Earthquake Spectra*, *29*(s1), 161–181.

Ghobarah, A., Saatcioglu, M., & Nistor, I. (2006). The impact of the 26 december 2004 earthquake and tsunami on structures and infrastructure. *Engineering structures*, *28*(2), 312–326.

Hayashi, S., & Koshimura, S. (2013). The 2011 tohoku tsunami flow velocity estimation by the aerial video analysis and numerical modeling. *Journal of Disaster Research*, *8*(4), 561–572.

Hirano, M. (1971). River bed degradation with armoring. *Proceedings of Japan Society of Civil Engineers*, *1971*(195), 55–65.

Ian, G., & Yoshua, B. (2016). *Deep learning (adaptive computation and machine learning)*. MIT Press, Cambridge.

Imamura, F., Boret, S. P., Suppasri, A., & Muhari, A. (2019). Recent occurrences of serious tsunami damage and the future challenges of tsunami disaster risk reduction. *Progress in Disaster Science*, *1*, 100009.

Jaffe, B., & Gelfenbuam, G. (2007). A simple model for calculating tsunami flow speed from tsunami deposits. *Sedimentary Geology*, *200*(3), 347–361.

Jaffe, B., Goto, K., Sugawara, D., Gelfenbaum, G., & La Selle, S. (2016). Uncertainty in tsunami sediment transport modeling. *Journal of Disaster Research*, *11*(4), 647–661.

Jaffe, B., Goto, K., Sugawara, D., Richmond, B., Fujino, S., & Nishimura, Y. (2012). Flow speed estimated by inverse modeling of sandy tsunami deposits: results from the 11 march 2011 tsunami on the coastal plain near the sendai airport, honshu, japan. *Sedimentary Geology*, *282*, 90–109.

Johnson, J. P., Delbecq, K., Kim, W., & Mohrig, D. (2016). Experimental tsunami deposits: Linking hydrodynamics to sediment entrainment, advection lengths and downstream fining. *Geomorphology*, *253*, 478–490.

Jordan, M. I., & Rumelhart, D. E. (1992). Forward models: Supervised learning

with a distal teacher. *Cognitive science*, *16*(3), 307–354.

Le, T. A., Baydin, A. G., Zinkov, R., & Wood, F. (2017). Using synthetic data to train neural networks is model-based reasoning. In *2017 international joint conference on neural networks (ijcnn)* (pp. 3514–3521).

Li, L., Qiu, Q., & Huang, Z. (2012). Numerical modeling of the morphological change in lhok nga, west banda aceh, during the 2004 indian ocean tsunami: understanding tsunami deposits using a forward modeling method. *Natural Hazards*, *64*(2), 1549–1574.

Lin, A., Ikuta, R., & Rao, G. (2012). Tsunami run-up associated with co-seismic thrust slip produced by the 2011 mw 9.0 off pacific coast of tohoku earthquake, japan. *Earth and Planetary Science Letters*, *337*, 121–132.

Moore, A., McAdoo, B. G., & Ruffman, A. (2007, 08). Landward fining from multiple sources in a sand sheet deposited by the 1929 grand banks tsunami, newfoundland. *Sedimentary Geology*, *200*, 336-346.

Mori, N., Takahashi, T., & Group, . T. E. T. J. S. (2012). Nationwide post event survey and analysis of the 2011 tohoku earthquake tsunami. *Coastal Engineering Journal*, *54*(1), 1250001–1.

Nakajima, H., & Koarai, M. (2011). Assessment of tsunami flood situation from the great east japan earthquake. *Bull Geospatial Info Authority Japan*, *59*, 55–66.

Naruse, H., & Abe, T. (2017). Inverse tsunami flow modeling including nonequilibrium sediment transport, with application to deposits from the 2011 tohoku-oki tsunami. *Journal of Geophysical Research: Earth Surface*, *122*(11), 2159–2182.

Nisbet, R., Elder, J., & Miner, G. (2009). *Handbook of statistical analysis and data mining applications*. Academic Press.

Patterson, J., & Gibson, A. (2017). *Deep learning: A practitioner's approach*. " O'Reilly Media, Inc.".

Quenouille, M. (1949, 01). Approximate tests of correlation in time-series. *Journal of the Royal Statistical Society B*, *11*, 68-84.

Rijn, L. C. v. (1984). Sediment transport, part ii: suspended load transport. *Journal of hydraulic engineering*, *110*(11), 1613–1641.

Romano, M., Liong, S.-Y., Vu, M. T., Zemskyy, P., Doan, C. D., Dao, M. H., & Tkalich, P. (2009). Artificial neural network for tsunami forecasting. *Journal*

of Asian Earth Sciences, *36*(1), 29–37.

Saatcioglu, M., Ghobarah, A., & Nistor, I. (2005). Effects of the december 26, 2004 sumatra earthquake and tsunami on physical infrastructure. *ISET J. Earthq. Technol*, *42*, 79–94.

Shephard, F., Macdonald, G., & Cox, D. (1950). The tsunami of april, 1946. *Scripps Inst. Oceanog. Bull*, *5*(6), 391–528.

Smith, D., Foster, I. D., Long, D., & Shi, S. (2007). Reconstructing the pattern and depth of flow onshore in a palaeotsunami from associated deposits. *Sedimentary Geology*, *200*(3-4), 362–371.

Smith, J., & Eli, R. N. (1995). Neural-network models of rainfall-runoff process. *Journal of water resources planning and management*, *121*(6), 499–508.

Smith, S. (2013). *Digital signal processing: a practical guide for engineers and scientists*. Elsevier.

Soulsby, R. (1997). Dynamics of marine sands thomas telford publications. *London, UK*.

Soulsby, R., Smith, D., & Ruffman, A. (2007). Reconstructing tsunami run-up from sedimentary characteristics—a simple mathematical model. In (Vol. 7, pp. 1075–1088).

Srivastava, N., Hinton, G., Krizhevsky, A., Sutskever, I., & Salakhutdinov, R. (2014). Dropout: a simple way to prevent neural networks from overfitting. *The journal of machine learning research*, *15*(1), 1929–1958.

Sugawara, D. (2014). Extracting magnitude information from tsunami deposits. *JOURNAL OF GEOGRAPHY-CHIGAKU ZASSHI*, *123*(6), 797–812.

Sugawara, D., Goto, K., Imamura, F., Matsumoto, H., & Minoura, K. (2012). Assessing the magnitude of the 869 jogan tsunami using sedimentary deposits: Prediction and consequence of the 2011 tohoku-oki tsunami. *Sedimentary Geology*, *282*, 14–26.

Sutskever, I., Martens, J., Dahl, G., & Hinton, G. (2013). On the importance of initialization and momentum in deep learning. In *International conference on machine learning* (pp. 1139–1147).

Tang, H., Wang, J., Weiss, R., & Xiao, H. (2018). Tsuflind-enkf: Inversion of tsunami flow depth and flow speed from deposits with quantified uncertainties. *Marine Geology*, *396*, 16–25.

924 Tang, H., & Weiss, R. (2015). A model for tsunami flow inversion from deposits
925 (TSUFLIND). *Marine Geology*, *370*, 55–62.
926 Tobin, J., Fong, R., Ray, A., Schneider, J., Zaremba, W., & Abbeel, P. (2017). Do-
927 main randomization for transferring deep neural networks from simulation to
928 the real world. In *2017 ieee/rsj international conference on intelligent robots*
929 *and systems (iros)* (pp. 23–30).
930 Tremblay, J., Prakash, A., Acuna, D., Brophy, M., Jampani, V., Anil, C., ... Birch-
931 field, S. (2018). Training deep networks with synthetic data: Bridging the
932 reality gap by domain randomization. In *Proceedings of the ieee conference on*
933 *computer vision and pattern recognition workshops* (pp. 969–977).
934 Yoshii, T., Tanaka, S., & Matsuyama, M. (2018). Tsunami inundation, sediment
935 transport, and deposition process of tsunami deposits on coastal lowland in-
936 ferred from the tsunami sand transport laboratory experiment (tstle). *Marine*
937 *Geology*, *400*, 107–118.
938 Yoshikawa, Y., & Watanabe, Y. (2008). Examine of Manning's coefficient and the
939 bed-load layer for one-dimensional calculation of bed variation. *Monthly Report*
940 *of Civil Engineering Research Institute for Cold Region*, *662*, 11–20.